



1

2 **Summer surface air temperature proxies point to near sea-ice-free conditions in the Arctic at**
3 **127 ka.**

4

5 Louise C. Sime¹, Rahul Sivankutty¹, Irene Vallet-Malmierca¹, Agatha M. de Boer², and Marie Sicard²

6 ¹British Antarctic Survey, Cambridge, UK

7 ²Department of Geological Sciences, Stockholm University, Sweden.

8

9 Correspondence: Louise C. Sime (lsim@bas.ac.uk)

10



11 **Abstract.**

12 The Last Interglacial (LIG) period, which had higher summer solar insolation than today, has been
13 suggested as the last time that Arctic summers were ice-free. However, the latest suite of Coupled
14 Modelling Intercomparison Project 6 Paleoclimate (CMIP6-PMIP4) simulations of the LIG produce a
15 wide range of Arctic summer minimum sea ice area (SIA) results, ranging from a 30% to 96%
16 reduction from the pre-industrial (PI). Sea ice proxies are also currently neither abundant nor
17 consistent enough to determine the most realistic state. Here we estimate LIG minimum SIA
18 indirectly through the use of 21 proxy records for LIG Summer Surface Air Temperature (SSAT) and
19 11 CMIP6-PMIP4 models for the LIG. We use two approaches. First, we use two tests to determine
20 how skilful models are at simulating observed proxies for Δ SSAT (where Δ refers to LIG-PI). This
21 identifies a positive correlation between model skill and the magnitude of Δ SIA: the most reliable
22 models simulate a larger sea ice reduction. Averaging the most skilful two models yields an average
23 SIA of 1.3 mill. km² for the LIG. This equates to a 4.5 mill. km², or a 79%, SIA reduction from the PI
24 to the LIG. Second, across the 11 models, the averaged Δ SSAT at the 21 proxy locations is inversely
25 correlated with Δ SIA ($r = -0.86$). In other words, the models show that a larger Arctic warming is
26 associated with a greater sea ice reduction. Using the proxy record-averaged Δ SSAT of 4.5 ± 1.7 K
27 and the relationship between Δ SSAT and Δ SIA, suggests an estimated Δ SIA of 4.4 mill. km² or 77%
28 less than the PI. The mean proxy-location Δ SSAT is well-correlated with the Arctic-wide Δ SSAT
29 north of 60°N ($r=0.97$) and this relationship is used to show that the mean proxy record Δ SSAT is
30 equivalent to an Arctic-wide warming of 3.7 ± 0.1 K at the LIG compared to the PI. Applying this
31 Arctic-wide Δ SSAT and its modelled relationship to Δ SIA, results in a similar estimate of LIG sea ice
32 reduction of 4.5 mill. km². The LIG climatological minimum SIA of 1.3 mill. km² is close to the
33 definition of a summer ice-free Arctic, which is a maximum sea ice extent less than 1 mill. km². The
34 results of this study thus suggest that the Arctic likely experienced a mixture of ice-free and near ice-
35 free summers during the LIG.

36



37 **1. Introduction**

38 The rapid decline in Arctic sea ice over the last 40 years is an icon of contemporary climate change.
39 Climate models have struggled to fully capture this sea ice loss (Notz and Community, 2020), which
40 can sometimes reduce confidence in their future projections (*e.g.* IPCC, 2021). One line of
41 investigation to address this problem, that has not been fully exploited, is the use of past climates to
42 provide information on the future (*e.g.* Bracegirdle et al., 2019). Investigating the physics and causes
43 of sea ice change, concentrating on Arctic changes during the most recent warm climate periods can
44 help us address this problem (Guarino et al., 2020b). Interglacials are periods of globally higher
45 temperatures which occur between cold glacial periods (Sime et al., 2009; Otto-Bliesner et al., 2013;
46 Fischer et al., 2018). The differences between colder glacial and warmer interglacial periods are
47 driven by climate feedbacks alongside changes in the Earth's orbit which affect incoming radiation.
48 The Last Interglacial or LIG, occurred 130,000-116,000 years ago. At 127,000 years ago, at high
49 latitudes orbital forcing led to summertime top-of-atmosphere shortwave radiation $60\text{--}75\text{ Wm}^{-2}$
50 greater than the PI period. Summer temperatures in the Arctic during the LIG are estimated to be
51 around 4.5 K above those of today (CAPE members, 2006; Kaspar et al., 2005; IPCC, 2013; Capron
52 et al., 2017). Prior to 2020, most climate models simulated summer LIG temperatures which were too
53 cool compared with these LIG temperature observations (Otto-Bliesner et al., 2013; IPCC, 2013).
54 This led Lunt et al. (2013); Otto-Bliesner et al. (2013) and IPCC (2013) to suggest that the
55 representation of dynamic vegetation changes in the Arctic might be key to understanding LIG
56 summertime Arctic warmth.

57

58 Guarino et al. (2020b) argued that loss of Arctic sea-ice in the summer could cause the warm summer
59 Arctic temperatures, without the need for dynamic vegetation. Using the HadGEM3 model, which
60 was the UK's contribution for the LIG CMIP6-PMIP4 project, Guarino et al. (2020b) found that the
61 model simulated a fully sea ice-free Arctic during the summer, *i.e.* it had less than 1 mill. km² of sea
62 ice extent at its minimum. This unique, near complete, loss of summer sea ice appears to happen in
63 the UK model, because it includes a highly advanced representation of melt ponds (Guarino et al.
64 2020b; Diamond et al. 2021). These are shallow pools of water which form on the surface of Arctic



65 sea ice and which determine how much sunlight is absorbed or reflected by the ice (Guarino et al.,
66 2020b).

67

68 Malmierca-Vallet et al. (2018) found the signature of summertime Arctic sea ice loss in Greenland ice
69 cores. Kageyama et al. (2021) then led the international community in compiling all available marine
70 core Arctic sea ice proxy data for the LIG and testing it against CMIP6-PMIP4 simulations. The
71 Kageyama et al. (2021) synthesis of ocean core-based proxy records of LIG Arctic sea-ice change,
72 like Malmierca-Vallet et al. (2018), showed that compared to the PI it is very likely that Arctic sea ice
73 was reduced. However, Kageyama et al. (2021) also showed that directly determining sea-ice changes
74 from marine core data is difficult. The marine core observations suffer some conflicting
75 interpretations of proxy data sometimes from the same core, and imprecision in dating materials to the
76 LIG period in the high Arctic. Thus, determining the mechanisms and distribution of sea ice loss
77 during the LIG by directly inferring sea ice presence (or absence) from these preserved biological data
78 alone is not possible (Kageyama et al., 2021).

79

80 The Coupled Model Intercomparison Project Phase 6 (CMIP6) Paleoclimate Model Intercomparison
81 Project Phase (PMIP4) or CMIP6-PMIP4 LIG experimental protocol prescribes differences between
82 the LIG and PI in orbital parameters, as well as differences in trace greenhouse gas concentrations
83 (Otto-Bliesner et al., 2017). This standardised climate modelling protocol is therefore an ideal
84 opportunity for the community to use models to explore the causes of Arctic warmth using multi-
85 model approaches. In particular, it offers the opportunity to address the questions of whether the
86 Arctic sea ice loss is sufficient to explain LIG summertime temperature observations, or whether the
87 Arctic vegetation changes idea (Lunt et al., 2013; Otto-Bliesner et al., 2013; IPCC, 2013), is still
88 potentially required.

89

90 Guarino et al. (2020b) showed that the HadGEM3, the only CMIP-PMIP4 model with an ice-free
91 Arctic at the LIG, has an excellent match with observed Arctic air temperature in summer. The
92 average Δ SSAT in HadGEM3, for all locations with proxy observations, is $+4.9 \pm 1.2$ K compared



93 with the observational mean of $+4.5 \pm 1.7$ K. This model also matched all, except one, marine core
94 sea-ice datapoints from Kageyama et al. (2021). Here we investigate whether there are more CMIP6-
95 PMIP4 models with a similarly good Δ SSAT and if so, whether other models with a good match also
96 suggest a much-reduced sea ice area (SIA) during the LIG. We further compute the correlation and
97 linear relationship in the models between Δ SSAT and Δ SIA and subsequently use this equation and
98 proxies for Δ SSAT to estimate Δ SIA. Section 2 describes the proxy data and models used in this
99 study as well as the analysis methods. The results are presented in Section 3 which first evaluates the
100 modelled PI and LIG sea ice distribution against observations and then use the above described
101 approaches to estimate the sea ice reduction at the LIG. Section 4 summarises the results and
102 discusses their shortcomings and implications.

103

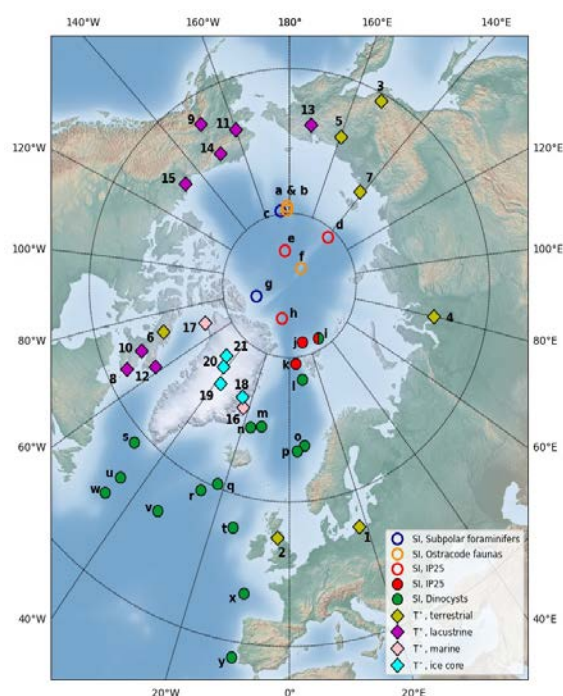
104 **2. Data and methods**

105 **2.1 Observational data**

106 The LIG SSAT proxy observations used to assess LIG Arctic sea ice in the Guarino et al. (2020b)
107 study were previously published by CAPE members (2006); Kaspar et al. (2005) and 20 of them were
108 also used to assess CMIP5 models in the IPCC (2013) report. A detailed description of each
109 observation is available (CAPE members, 2006; Kaspar et al., 2005; IPCC, 2013; Capron et al.,
110 2017). Each observation is thought to be of summer LIG air temperature anomaly relative to present
111 day and is located in the circum-Arctic region; all sites are from north of 51° N. There are 7 terrestrial
112 based temperature records; 8 lacustrine records; 2 marine pollen-based records; and 3 ice core records
113 included in the original IPCC (2013) compilation. Guarino et al. (2020b) added to this an additional
114 new observation from the NEEM Greenland ice core from Capron et al. (2017), bringing the total
115 number of proxies records to 21 (Table 1). Figure 1 shows the location, and type, for each numbered
116 observation. Whilst the exact timing of this peak warmth has not yet been definitively determined, it
117 is reasonable to assume that these measurements are approximately synchronous across the Arctic. It
118 is however very unlikely that the peak warmth was synchronous across both hemispheres (see Capron
119 et al. (2014); Govin et al. (2015)), and further investigation of the synchronicity of peak warmth



120 occurs across the Northern Hemisphere is merited. For consistency with modelled data, temperature
121 anomalies computed against present day conditions (i.e. 1961-1990 baseline) were corrected to
122 account for a +0.4K of global warming between PI (1850) and present day (1961-1990) conditions
123 (Turney and Jones, 2010). Therefore, Table 1 and Guarino et al. (2020b) values differ slightly (+0.4K)
124 from the original datasets so that they represent temperature anomalies relative to the PI.
125



126
127 *Figure 1: Map of data locations numbered to match Table 1. This combines the Kageyama et al.*
128 *(2021) sea ice locations 1 to 20 alongside with the temperature proxies from Table 1.*

129 Most of the sites have temperature uncertainty (one standard deviation) estimates, which are provided
130 in the Table 1. However, for 9 sites, the standard deviation of the temperature data was not available.
131 A standard deviation of $\pm 0.5\text{K}$ was used to account for this missing uncertainty: this is the smallest
132 standard deviation found in any proxy record across all sites, and is thus as a conservative estimation
133 of the uncertainty associated to proxy data (Guarino et al., 2020b).



134

135 *Table 1: Compilation of LIG-PI summertime surface air temperature (SSAT) anomalies used by*
 136 *Guarino et al. (2020b).*

| Number | Lat | Lon | Site | Observation type | Observation (K) |
|--------|-------|--------|----------------------|--|-----------------|
| 1 | 55 | 18 | Europe | Terrestrial: pollen, plant macrofossils | 3.4 ± 0.5 |
| 2 | 55 | -3 | UK | Terrestrial: Pollen, plant macrofossils | 2.4 ± 0.5 |
| 3 | 61 | 152.5 | Magadan | Terrestrial: pollen | 6.4 ± 2 |
| 4 | 68 | 80 | West-central Siberia | Terrestrial: pollen, plant macrofossils | 5.4 ± 2 |
| 5 | 68 | 160 | Northeast Siberia | Terrestrial: pollen | 6.4 ± 2 |
| 6 | 70 | -72.5 | Flitaway | Terrestrial: insects, plant remains | 4.9 ± 0.5 |
| 7 | 73.33 | 141.5 | Bolshoy Lyadhovshy | Terrestrial: pollen | 4.9 ± 0.5 |
| 8 | 63 | -66 | Robinson Lake | Lacustrine: pollen | 5.4 ± 0.5 |
| 9 | 64 | -150 | Birch Creek/ky11 | Lacustrine: pollen | 1.4 ± 1 |
| 10 | 66 | -69.2 | Amarok Lake | Lacustrine: pollen | 4.9 ± 0.5 |
| 11 | 67 | -160 | Squirrel Lake | Lacustrine: pollen, plant macrofossils | 1.9 ± 1.5 |
| 12 | 67 | -62 | Cumber | Lacustrine: pollen | 5.9 ± 1.5 |
| 13 | 67.5 | 172.08 | Lake Elgygytgyn | Lacustrine: pollen | 3.4 ± 1 |
| 14 | 69 | -151 | Ahaliorak Lake | Lacustrine: pollen | 1.9 ± 1.5 |
| 15 | 69 | -133 | Lake Tuk 5 | Lacustrine: plant macrofossils and beetles | 2.4 ± 0.5 |
| 16 | 71.75 | -23 | Jameson | Marine: pollen, plant macrofossils, beetles, other invertebrates | 5.4 ± 0.5 |
| 17 | 76.35 | -68.3 | Thule | Marine: pollen, chironomids | 4.4 ± 0.5 |
| 18 | 73 | -25 | Renland | Ice core: d18O, dD | 5.4 ± 0.5 |
| 19 | 73 | -38 | GISP2 | Ice core: d18O, dD | 5.4 ± 0.5 |
| 20 | 75 | -42 | NGRIP | Ice core: d18O, dD | 5.4 ± 0.5 |
| 21 | 76.4 | -44.8 | NEEM(ds) | Ice core: d18O, dD | 8 ± 4 |
| 137 | - | - | Arctic | Mean of observations 1 to 21 | 4.5 ± 1.7 |

138

139 2.2. Models and model output

140 We analyse Tier 1 LIG simulations, based on the standard CMIP6-PMIP4 LIG experimental protocol
 141 (Otto-Bliesner et al., 2017). The prescribed LIG (127 ka) protocol differs from the CMIP6 PI
 142 simulation protocol in astronomical parameters and the atmospheric trace GHG concentrations. LIG
 143 astronomical parameters are prescribed according to orbital constants (Berger and Loutre, 1991), and



144 atmospheric trace GHG concentrations are based on ice core measurements: 275 ppm for CO₂; 685
145 ppb for CH₄; and 255 ppb for N₂O (Otto-Bliesner et al., 2017).

146

147 The CMIP6-PMIP4 model simulations were run following the Otto-Bliesner et al. (2017) protocol,
148 except CNRM-CM6-1, which used GHG at their PI values rather than using LIG values. For all
149 models, all other boundary conditions, including solar activity, ice sheets, aerosol emissions etc., are
150 identical to the PI simulation. In terms of the Greenland and Antarctica ice sheets, a PI configuration
151 for the LIG simulation is not unreasonable (Kageyama et al., 2021; Otto-Bliesner et al., 2020). LIG
152 simulations were initialized either from a previous LIG run, or from the standard CMIP6 protocol PI
153 simulations, using constant 1850 GHGs, ozone, solar, tropospheric aerosol, stratospheric volcanic
154 aerosol and land use forcing. Whilst PI and LIG spin-ups vary between the models, with CNRM the
155 shortest at 100 years, most model groups aimed to allow the land and oceanic masses to attain
156 approximate steady state *i.e.* to reach atmospheric equilibrium and to achieve an upper-oceanic
157 equilibrium - which generally seems to take around 300 to 400 years. LIG production runs are all
158 between 100-200 years long, which is an appropriate length for Arctic sea ice analysis (Guarino et al.,
159 2020a).

160

161 Whilst fifteen models have run the CMIP6-PMIP4 LIG simulation (Kageyama et al., 2021; Otto-
162 Bliesner et al., 2020), and have uploaded model data to the Earth System Grid Federation (ESGF), we
163 exclude four simulations for the following reasons. The AWI-ESM and Nor-ESM models have LIG
164 simulations with two versions of model. To avoid undue biasing of results, we include only the
165 simulation from the latest version for each model. Additionally, for INM-CM4-8 model, no ocean or
166 sea ice fields were available for download, excluding this model from our analysis. Finally, we
167 exclude the CNRM model in the analysis because apart from using PI instead of LIG GHG
168 concentrations and a short spin-up time, the model also has known issues with its sea-ice model. The
169 model produces much too thin sea ice in September and March compared with observational evidence
170 and the snow layer on the ice is considerably overestimated (Voldoire et al., 2019). As a possible
171 consequence of these issues, the CNRM model is also an outlier in an otherwise highly correlated



172 (inverse) relationship in the models between the LIG-PI albedo change over the Arctic sea-ice and the
173 LIG-PI SSAT change over the ice, being the only model that produces a warmer LIG with almost no
174 reduction in albedo (Figure A1). While we consider the CNRM ice model unreliable for this study, we
175 note that the inclusion of the model in our analysis only reduces the correlation coefficients but does
176 not change the overall conclusions.

177

178 We thus analyse the difference between the PI and LIG simulations from eleven models. Out of the
179 eleven simulations of the LIG, seven have 200 years simulation length (data available to download in
180 ESGF), the remaining four are 100 years in length. For PI control runs, we use the last 200 years of PI
181 control run available in ESGF for each model. Details of each model: model denomination, physical
182 core components, horizontal and vertical grid specifications, details on prescribed vs interactive
183 boundary conditions, details of published model description, and LIG simulation length (spin-up and
184 production runs) are contained in (Kageyama et al., 2021). Data was downloaded from the ESGF data
185 node: <https://esgf-node.llnl.gov/projects/esgf-llnl/> (last downloaded on 23rd June 2021).

186

187 The spatial distribution of sea ice is usually computed in two ways, by its total area or its extent. The
188 sea ice extent (SIE) is the total area of the Arctic ocean where there is at least 15% ice concentration.
189 The total sea ice area (SIA) is the sum of the sea ice concentration times the area of a grid cell for all
190 cells that contain some sea ice. In this paper, the SIA refers to the SIA of the month of minimum sea
191 ice, as computed by using the climatology of the whole simulation.

192

193 **2.3. Assessing model skill to simulate reconstructions of Δ SSAT**

194 The model skill is quantified using two measures based on 1) the percentage of the 21 proxies for
195 Δ SSAT (in Table 1) for which the model produce a value within the error bars, and 2) the Root Mean
196 Square Error (RMSE) of the modelled SSAT compared to the proxies. To assess whether the model
197 match a proxy point, we compute summer mean (June to August) surface air temperatures for every
198 year for the PI and LIG for each model. Climatological summer temperature is the time mean of these



199 summer temperatures for the entire simulation length. Our calculated model uncertainties on the
200 climatological summer mean temperatures are one standard deviation of summer mean time series for
201 each model. Bilinear interpolation in latitude-longitude space was used to extract values at the
202 observation locations from the gridded model output. For climatological summer mean temperature, if
203 there is an overlap between observation SSAT (plus observational uncertainty) and the simulated
204 SSAT (plus model uncertainty) then, for that location, the result is considered as a match. Similarly,
205 the RMSE error is calculated using the modelled SSAT values averaged over the summer months of
206 the entire simulation length.

207

208 **3. Results**

209 **3.1. Simulated Arctic sea ice distribution**

210 The sea ice distribution in the models have been reported previously in Kageyama et al. (2021) and is
211 included here to make this work self-reliant. For the PI, the model mean value for summer minimum
212 monthly SIA is 6.4 mill. km². Due to a lack of direct observations for the PI, the PI model results are
213 compared with observed 1981 to 2002 satellite observations, keeping in mind that the modern
214 observations are for a climate with a higher atmospheric CO₂ level of ~380 ppm, compared to the PI
215 atmospheric CO₂ levels of 280 ppm. The modern observed mean minimum SIA is 5.7 mill km²
216 (Reynolds et al., 2002). In general, the simulations show a realistic representation of the geographical
217 extent for the summer minimum. More models show a slightly smaller area compared to the present-
218 day observations, however EC-Earth, FGOALS-g3, and GISS170 E2-1-G simulate too much ice
219 (Figure 2). Overestimations appear to be due to too much sea ice being simulated in the Barents-Kara
220 area (FGOALS-g3, GISS-E2-1-G), in the Nordic Seas (EC-Earth, FGOALS-g3) and in Baffin Bay
221 (EC-Earth). Kageyama et al. (2021) also note that MIROC-ES2L performs rather poorly for the PI,
222 with insufficient ice close to the continents. The other models have a relatively close match to the
223 15% isoline in the NOAA Optimum Interpolation version 2 data (Reynolds et al., 2002; Kageyama et
224 al., 2021).

225



226 For the LIG, the model output is compared against the LIG sea ice synthesis of Kageyama et al.
227 (2021), which include marine cores collected in the Arctic Ocean, Nordic Seas and northern North
228 Atlantic (Figure 3). These data show that south of 79°N in the Atlantic and Nordic seas the LIG was
229 seasonally ice-free. These southern sea ice records provide quantitative estimates of sea surface
230 parameters based on dinoflagellate cysts (dinocysts). North of 79°N the sea-ice-related records are
231 more difficult to obtain and interpret. A core at 81.5°N brings evidence of summer being probably
232 seasonally ice-free during the LIG from two indicators: dinocysts and IP25/PIP25. However, an
233 anomalous core close by at the northernmost location of 81.9°N, with good chronology, shows IP25-
234 based evidence of substantial (> 75%) sea ice concentration all year round. Other northerly cores do
235 not currently have good enough chronological control to confidently date material of LIG age. All
236 models, except FGOALS, generally tend to match the results from proxies of summertime Arctic sea
237 ice in marine cores with good LIG chronology (Figure 3), apart from the anomalous northernmost
238 core for which the IP25 evidence suggest perennial sea ice (Kageyama et al., 2021). This may mean
239 that all the models tend to have similar problems in simulating Arctic sea ice during the LIG or that
240 the LIG IP25 signal in the Arctic indicates something else. What is clear is that a new approach with
241 other Arctic datasets, such as SSAT, may be needed to make progress on the LIG Arctic sea ice
242 question.

243

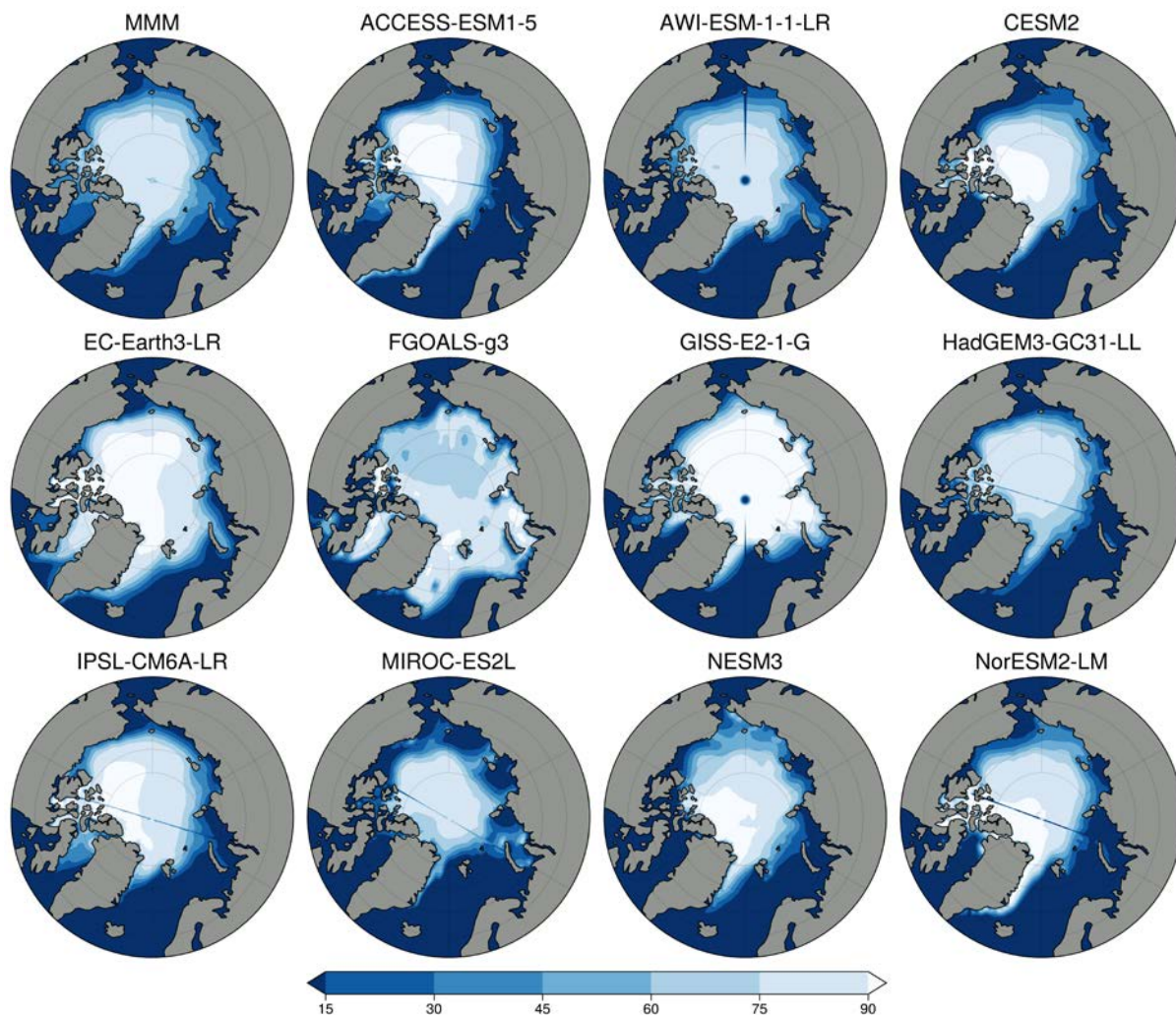
244

245

246

247

248



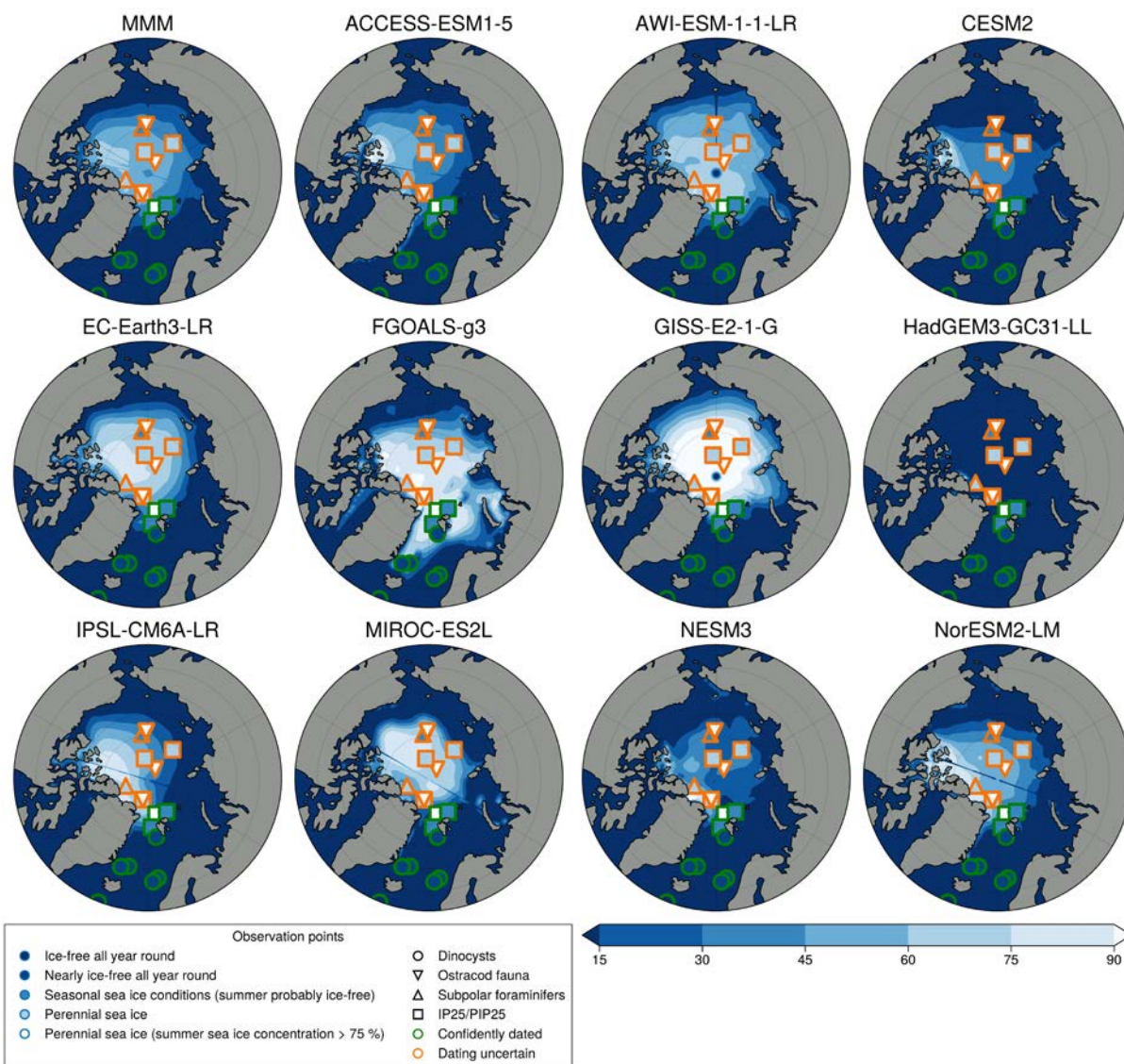
249

250

251

252 *Figure 2: Climatological Minimum PI sea ice concentration maps for each model. The first panel*
253 *represents the multi model mean (MMM).*

254



255
 256 *Figure 3: Climatological minimum LIG sea ice concentration maps for each model. Marine core*
 257 *results are from Kageyama et al. (2021); orange outlines indicate that the dating is uncertain; green*
 258 *outlines indicate the datapoint is from the LIG. The first panel represents the multi model mean.*

259



260 For the LIG, there is very little difference between the maximum (wintertime) Arctic SIA and that of
 261 the PI (which is 15-16 mill. km² between the PI and the LIG in most models), but every model shows
 262 a reduction in summer sea ice in the LIG compared to the PI (Table 2). Our model mean LIG
 263 summertime Arctic is 2.9 mill. km², compared to 6.4 mill. km² for the PI, or a 55% PI to LIG
 264 decrease. There is large inter-model variability for the LIG SIA during the summer (Figure 4). All
 265 models show a larger sea-ice area seasonal amplitude for LIG than for PI, and the range of model SIA
 266 is larger for LIG than for PI (Figure A2). The results for individual years show that no model is close
 267 to the ice-free threshold for any model summer during their PI simulation (Figure 4) but for the LIG
 268 summer SIA, there are three models which are lower than 1 mill. km² for at least one summer during
 269 the LIG simulation (Figure 4). Of these three, HadGEM3, shows a LIG Arctic Ocean free of sea ice in
 270 all summers, *i.e.* its maximum SIE is lower than 1 mill. km² in all LIG simulation years. CESM2 and
 271 NESM3 show low climatological SIA values (slightly above 2 mill. km²) in summer for the LIG
 272 simulation, and both have at least one year with a SIE minimum which is below 1 mill. km², though
 273 their average minimum SIE values are just below 3 mill. km². Of these low LIG sea ice models,
 274 HadGEM3 and CESM2 realistically capture the PI Arctic sea ice seasonal cycle, whilst NESM3
 275 overestimates winter ice and the amplitude of the seasonal cycle (Cao et al., 2018).

276

277 *Table 2: The minimum climatological sea ice area for the PI and the LIG, changes, and the*
 278 *associated Δ SSAT anomalies. Percentage reductions are calculated from PI minimum SIA for each*
 279 *model.*

| MODEL (units) | SIA PI (mill. km ²) | SIA LIG (mill. km ²) | ΔSIA (mill. km ²) | SIA (% loss) | ΔSSAT (K) |
|-------------------------|---|--|---|------------------------|---------------------------------------|
| MMM | 6.36 | 2.93 | -3.43 | 53.87 | 3.6±1.3 |
| ACCESS-ESM1-5 | 5.48 | 2.39 | -3.09 | 56.44 | 2.6±1 |
| AWI-ESM-1-1-LR | 5.37 | 3.76 | -1.61 | 29.99 | 1.7±1.1 |
| CESM2 | 5.31 | 1.62 | -3.69 | 69.54 | 3.3±1 |
| EC-Earth3-LR | 8.86 | 3.65 | -5.21 | 58.84 | 5.7±2.6 |
| FGOALS-g3 | 8.83 | 5.55 | -3.29 | 37.19 | 4.8±1.5 |



| | | | | | |
|-----------------|------|------|-------|-------|-----------|
| GISS-E2-1-G | 8.87 | 5.54 | -3.32 | 37.47 | 3.4±1.4 |
| HadGEM3-GC31-LL | 5.21 | 0.13 | -5.07 | 97.48 | 4.9±1.2 |
| IPSL-CM6A-LR | 6.42 | 2.46 | -3.96 | 61.74 | 4.4±1.2 |
| MIROC-ES2L | 4.20 | 2.79 | -1.41 | 33.66 | 2.1 ± 0.6 |
| NESM3 | 5.50 | 1.64 | -3.86 | 70.14 | 3 ±0.9 |
| NorESM2-LM | 5.92 | 2.75 | -3.17 | 53.52 | 3.6±1.1 |

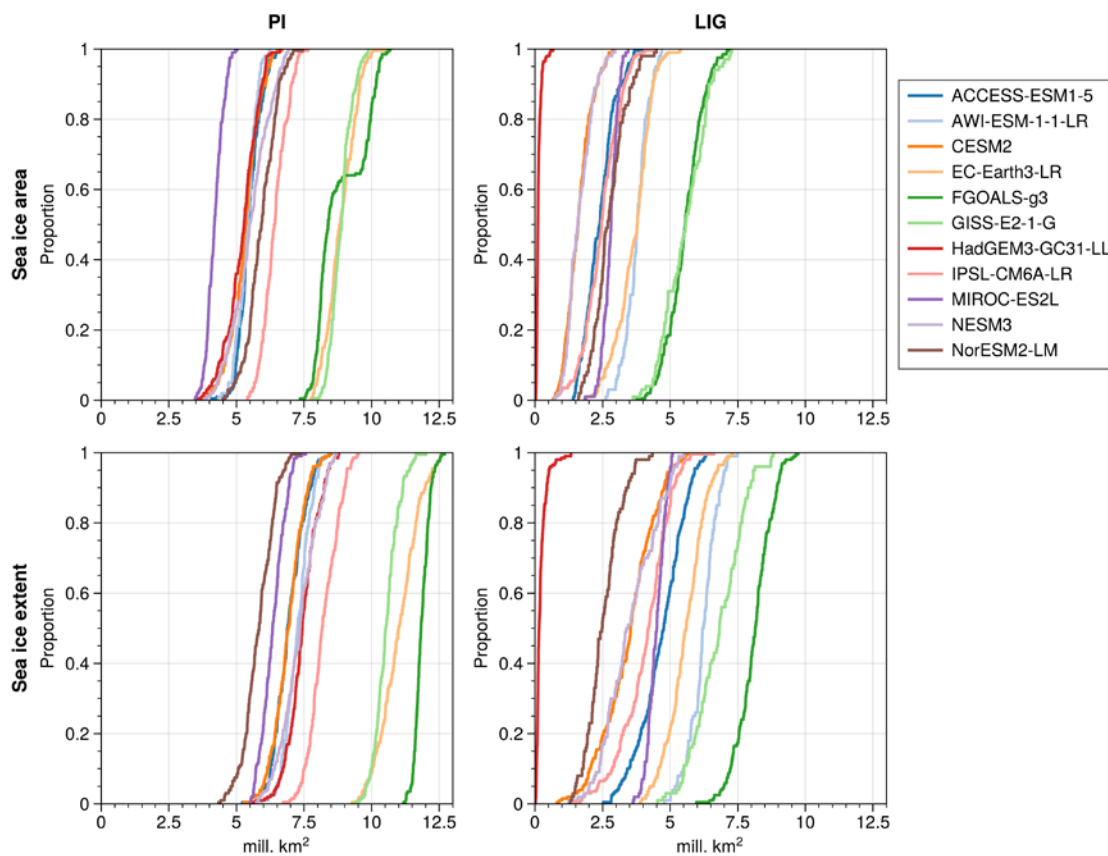


Figure 4: Cumulative distribution of minimum SIA of individual years in LIG and PI simulations, i.e SIA versus proportion of years which fall below the corresponding SIA value. HadGEM3 has minimum SIA below 1 mill km² for all years in LIG runs. CESM2 has 6.5%, and NESM3 8%, LIG years with SIA below 1 mill km². Lower Panels are same but for SIE.

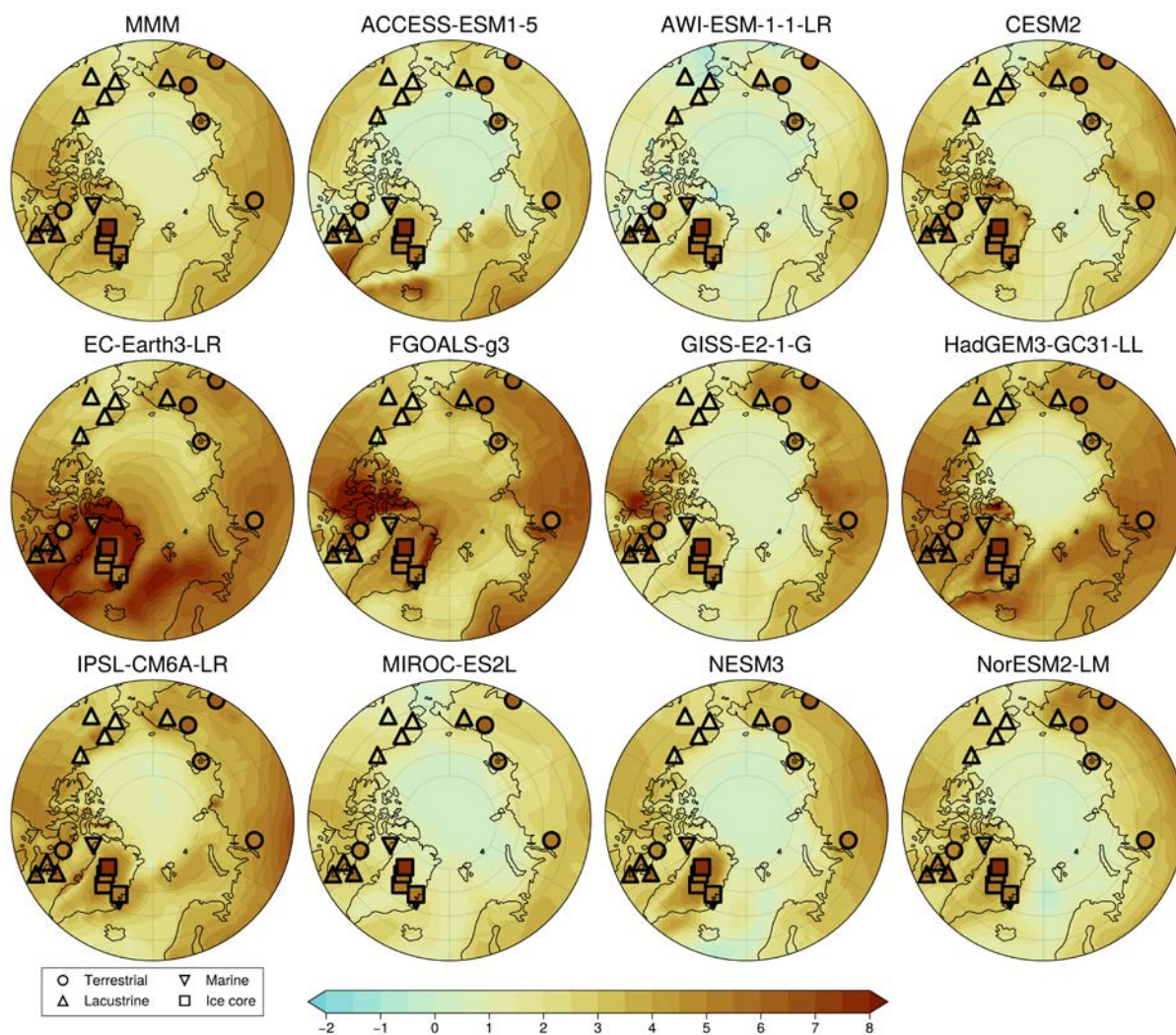


281 **3.2. Estimating Δ SIA from model skill to simulate Δ SSAT**

282 We first investigate whether there is a relationship between how well models match proxy Δ SSAT
283 and the magnitude of SIA reduction that they simulate for the LIG. A visual comparison of modelled
284 Δ SSAT and proxy estimates for Δ SSAT is also shown in Figure 5. As described in Section 2, two
285 different approaches are used to quantify the skill of the models to simulate Δ SSAT, based on 1) the
286 RMSE of the model-data Δ SSAT at the proxy record locations and 2) the percentage Δ SSAT proxies
287 that the model can correctly match, within model and data error. Here the focus is on quantifying
288 model skill across all data records, but for reference, the model-versus-proxy Δ SSAT for each
289 location is provided for each model individually in Figure A3. The RMSE skill estimate and the
290 percentage match estimate provide very similar indications of which models have good skill to
291 reproduce proxy Δ SSAT. The five models with the lowest RMSE also have the highest percentage
292 match and the two models with the highest RMSE have the lowest percentage match (Figure 6). Both
293 approaches show that the models with better skill to simulate Δ SSAT have a high absolute Δ SIA. The
294 only outlier is EC-Earth, which has an average skill (6th best model of 11) but a high SIA reduction at
295 the LIG. This occurs because the EC-Earth PI simulation has an excessive SIA, more than 3 million
296 km² compared with observations; this enables it to have a large Δ SIA value, whilst likely retaining too
297 much LIG SIA. Quantitatively there is a correlation of $r=-0.65$ ($p=0.03$) between the magnitude of
298 Δ SIA and the RMSE, and a correlation with $r=0.67$ ($p=0.02$) between the magnitude of Δ SIA and the
299 percentage match of the model (Figure 6). Given that the SIA reduction from the PI to the LIG could
300 be dependent on the starting SIA at the PI, we repeat the analysis for percentage SIA loss from the PI
301 (rather than absolute SIA loss) and find that it correlates similarly to the model skill to reproduce
302 Δ SSAT (Figure A4).

303

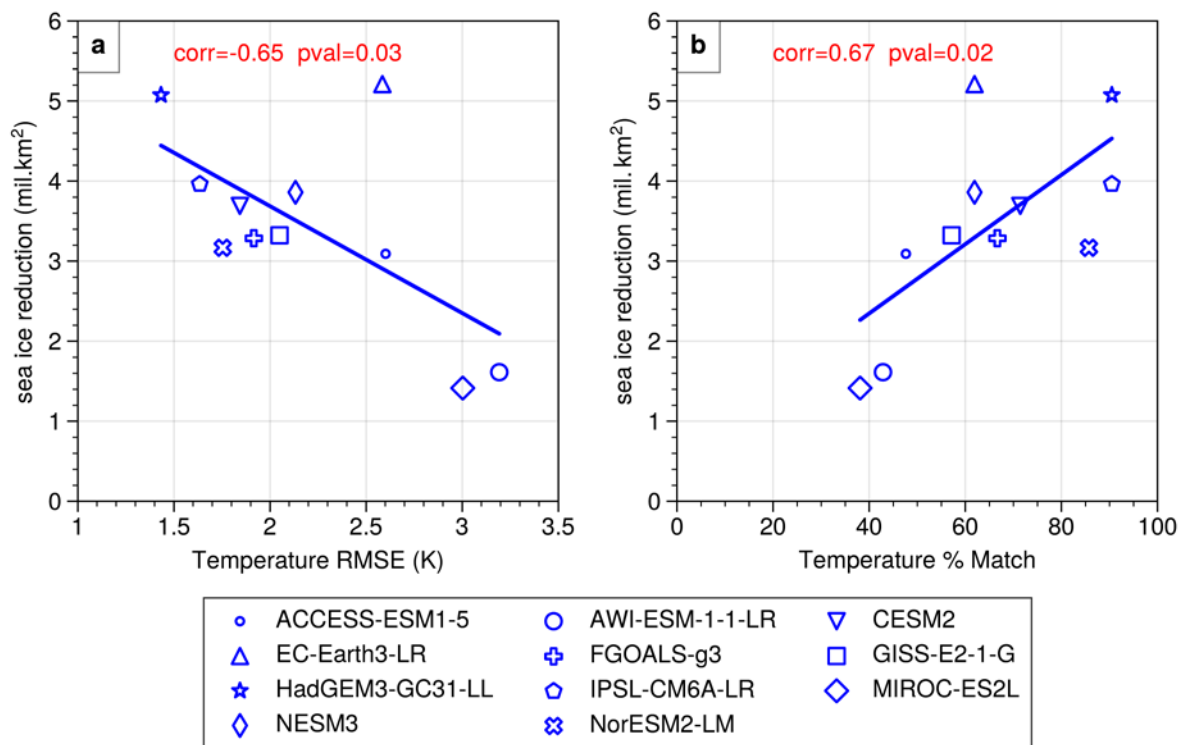
304



305

306 *Figure 5: Summertime surface air temperature (SSAT) anomaly (LIG - PI) maps for each model*
307 *overlayed by observed summer temperature anomalies. Proxies are detailed in Table 1 and Guarino et*
308 *al. (2020b); colours are the same as used for the underlying model data. The first panel represents the*
309 *multi model mean.*

310



311

312

313 *Figure 6: Modelled magnitude of ΔSIA versus model skill to simulate proxy $\Delta SSAT$. a) The modelled*
 314 *magnitude of ΔSIA is scattered against the RMS error of the modelled $\Delta SSAT$ compared to the proxy*
 315 *$\Delta SSAT$ for the 21 data locations. b) The modelled magnitude of ΔSIA scattered against the percentage*
 316 *of $\Delta SSAT$ data points that the model can match (see methods).*

317

318 In general, where models have a closer match with the $\Delta SSAT$, they have a higher absolute ΔSIA , as
 319 well as a larger percentage reduction of SIA from the PI. We thus look at our best performing models
 320 for an indication of true LIG Arctic sea ice reduction. The four models with the best agreement of
 321 $\Delta SSAT$ to proxies are in order of skill; HadGEM3, IPSL, NORESM2, and CESM2. The top two
 322 performing models simulate an average SIA loss of 4.5 mill. km² from an average starting PI SIA of
 323 5.8 mill. km² to a final LIG SIA of 1.3 mill. km², which equates to a percentage SIA loss of 79%.
 324 Including also the two next-best performing models in the average results in an average SIA loss of



325 4.0 mill. km² to a final LIG SIA of 1.7 mill. km² from an average starting PI SIA of 5.7 mill. km²,
326 which equates to a percentage SIA loss of 71%.

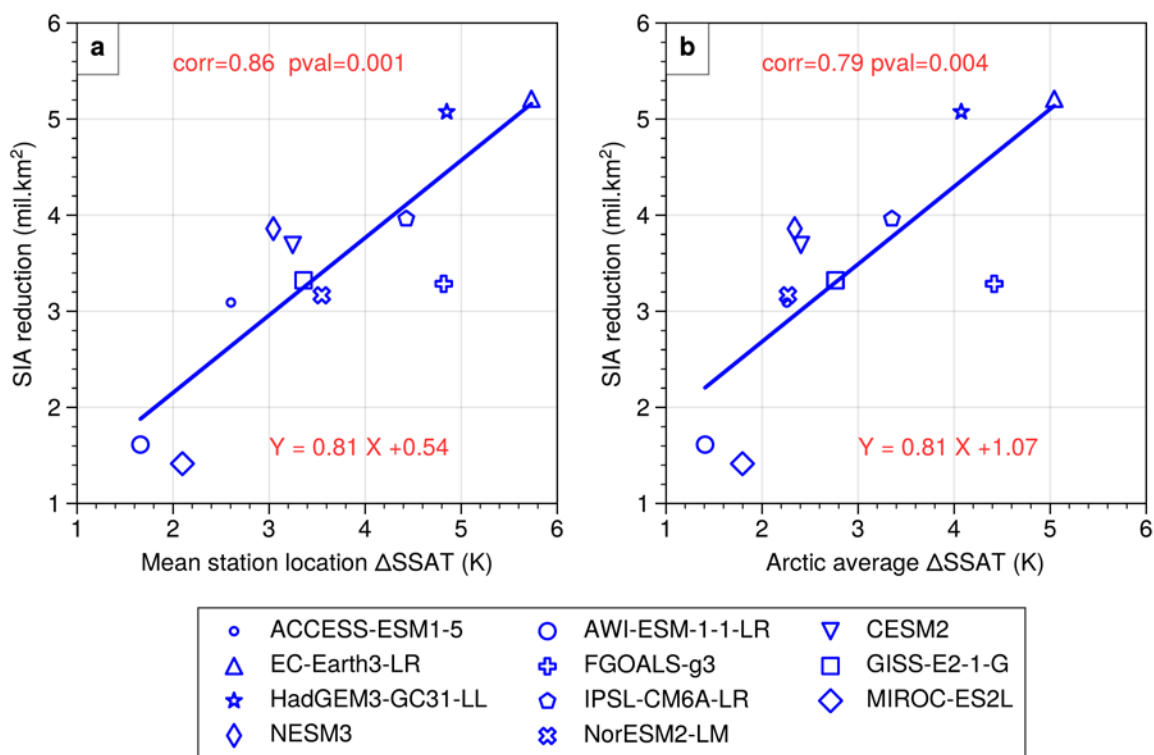
327

328 The question arises as to why there is a linear relationship between model skill to simulate Arctic
329 Δ SSAT and SIA reduction. One possibility is that the mean proxy Δ SSAT of 4.5 K is higher than
330 what most models produce, and that the warmer models are thus closer to the proxies and also more
331 likely to reduce sea ice. In the next section, this question is addressed by investigating whether Δ SIA
332 is closely related to Δ SSAT itself.

333

334 **3.3. Estimating Δ SIA from the modelled Δ SIA- Δ SSAT relationship and proxy Δ SSAT**

335 Here we investigate whether the models suggest a linear relationship between Δ SSAT and Δ SIA, and
336 if so, exploit that together with proxy Δ SSAT to estimate the most likely (true) value for Δ SIA. We
337 first calculate the mean Δ SSAT in the model at all 21 proxy data locations and compare it to the
338 magnitude of Δ SIA in each model (Figure 7a). The two are well correlated with $r=0.86$ ($p=0.001$) and
339 the regression equation provide a dependence of Δ SIA on Δ SSAT. Using this relation, the observed
340 mean Δ SSAT at the proxy locations points to a SIA reduction of 4.4 mill. km² from the PI. This
341 constitutes a 77% reduction from the present day observation of 5.7 mill. km², which is also the
342 average SIA for the PI in the two most skilful models identified in the previous section. Using this
343 value for the PI sea ice, suggests remaining minimum of 1.3 mill. km² of sea ice during the LIG
344 summer. An average LIG minimum of 1.3 mill. km² implies that some LIG summers must have been
345 ice-free (below 1 mill. km² in SIE) but that most summers would have had a small amount of sea ice.



346

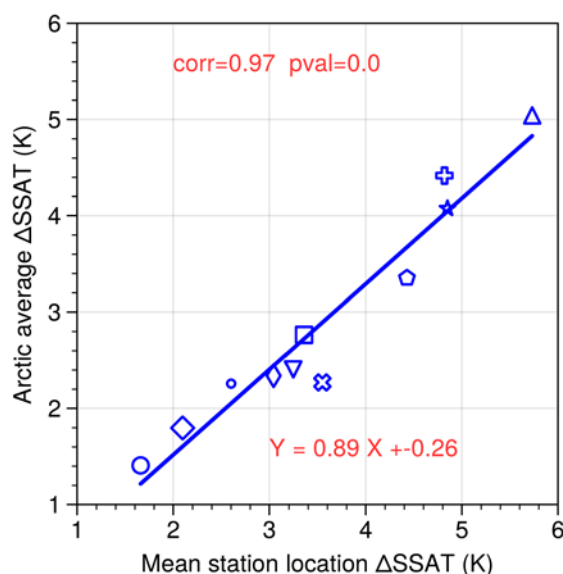
347 *Figure 7: Modelled magnitude of ΔSIA versus modelled $\Delta SSAT$ for the Arctic. a) The modelled ΔSIA*
 348 *is scattered against mean modelled $\Delta SSAT$ at the 21 data locations. b) The modelled ΔSIA is scattered*
 349 *against the mean modelled $\Delta SSAT$ averaged over the Arctic north of $60^\circ N$.*

350

351 The $\Delta SSAT$ relationship to ΔSIA has so far been computed using the mean $\Delta SSAT$ at the locations of
 352 the data. To test whether this method would also work for the Arctic in general, the $\Delta SSAT$ is next
 353 averaged over the whole Arctic north of $60^\circ N$ and compared with ΔSIA (Figure 7b). The correlation
 354 between $\Delta SSAT$ and ΔSIA is a somewhat reduced when calculating $\Delta SSAT$ across the whole Arctic,
 355 though it is still highly significant ($r=0.79$, $p=0.004$). An estimate for proxy-based Arctic-wide
 356 $\Delta SSAT$ can be derived by applying the close relationship between Arctic $\Delta SSAT$ and station $\Delta SSAT$
 357 in the models (Figure 8, $r=0.97$, $p < 0.001$). Inserting the $\Delta SSAT$ averaged over all proxy-records, of
 358 4.5 K, in the regression equation in Figure 8, gives an estimate for proxy-based Arctic-wide $\Delta SSAT$



359 of 3.7 ± 0.1 K. Applying the regression equation in Figure 7b and using this estimate for Arctic-wide
360 Δ SSAT suggests a PI to LIG sea ice reduction of 4.5 mill. km², which is very similar to the estimate
361 derived from the station data alone (of 4.4 mill. km²).
362



375 Figure 8: Modelled Arctic-wide Δ SSAT versus modelled mean Δ SSAT at the data locations for the 11
376 models.

377

378 4. Discussion and conclusions

379 As discussed in the introduction, neither proxies nor modelling results alone allow currently for a
380 convincing estimate of the Arctic sea ice reduction at the LIG. Here we apply a joint approach to
381 make progress. We deduce how much sea ice was reduced during the LIG, using 11 of the most recent
382 CMIP6-PMIP4 LIG model simulations and proxy observations of summer air temperature changes.
383 The reduction of sea ice from the PI to the LIG in the models range from 30% to 96% with an average
384 of 55%. No model is close to the ice-free threshold, of maximum SIE lower than 1 mill. km², for any
385 model year-summer during their PI simulation. During the LIG, the HadGEM3 model is the only one
386 that has an Arctic Ocean free of sea ice in all summers, although CESM2 and NESM3 show SIA

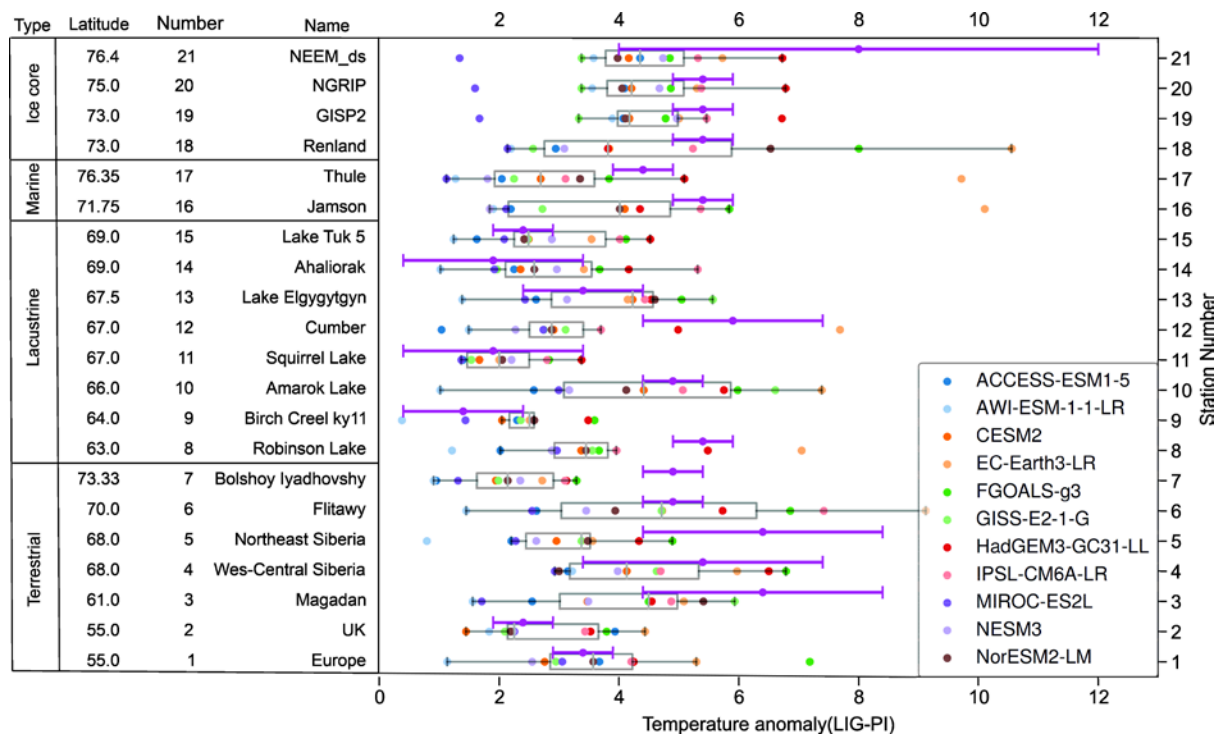


387 values of around 2 mill. km², in association with intermittently ice-free conditions. We found that
388 larger LIG SIA reduction from the PI is related to greater SSAT warming, the two being correlated
389 with $r=0.86$ across the models. In particular, the 8 models with largest SIA reduction are all able to
390 match, within uncertainty, the mean PI to LIG summertime Arctic warming of 4.5 ± 1.7 K at the 21
391 proxy locations. This magnitude of warming was difficult to reach with previous generations of LIG
392 models.

393
394 We find that the good match between the (ice-free) HadGEM3 and the Guarino et al. (2020b) summer
395 Arctic temperature dataset is not unique. However, we find that it is not random either and that there
396 is a correlation between model skill to match the Δ SSAT and the reduction of SIA from the PI to the
397 LIG (both when using an RMSE skill test and when using a best-match skill test). The two most
398 skilful models simulate an average LIG sea ice area of 1.3 mill. km² which is a 4.5 mill. km² or 79%
399 reduction from their PI values. Whilst we cannot assume all model error Δ SSAT is attributable to
400 Δ SIA, it is reasonable to assume that the better performing models for Δ SSAT are also better at
401 simulating Δ SIA, because of the close relationship between warming and sea ice loss.

402
403 Some of the proxies are more difficult for the models to simulate (Figure 9 and Figure A3). In
404 particular, it appears that the Greenland ice core SSAT value from NEEM of +8 K (observation 21 in
405 Table 1 Figure 9) is higher than any model simulates; though with a ± 4 K uncertainty it is
406 nevertheless matched by some models. Terrestrial proxies three and six, with SSAT values of +6.4 K
407 are also only rarely matched. Further work on the observational side would be useful. These LIG
408 SSAT proxy reconstructions were used in the IPCC (2013) report and by Guarino et al. (2020b); and
409 were previously published by IPCC (2013); CAPE members (2006); Kaspar et al. (2005); Capron et
410 al. (2017). Thus, this dataset should ideally be improved. One start point for this would be adding
411 uncertainties to the (nine) sites which do not currently have these numbers.

412



413

414 *Figure 9: Proxy ΔSSAT (violet dots and uncertainty bars) and simulated ΔSSAT for all models*
 415 *(coloured dots) for each proxy record location (rows). Grey boxes extend from the 25th to the 75th*
 416 *percentile of each locations distribution of simulated values and the vertical lines represent the*
 417 *median.*

418

419 The correlation between model skill to simulate ΔSSAT and the magnitude of ΔSIA is convincing ($r=$
 420 0.66 and $p= 0.003$ on average for the two skill tests). However, the two quantities are not
 421 straightforward to relate through a dynamical process. On the other hand, it is well known that there is
 422 a positive feedback between Arctic temperature and Arctic sea-ice, with warmer temperatures more
 423 likely to melt sea ice, and less sea ice producing a smaller albedo to incoming solar radiation and so
 424 less cooling from solar reflection. This dynamic is evident in the strong correlation of $r=0.86$ between
 425 the magnitude of ΔSIA and ΔSSAT. The reconstructed ΔSSAT from proxies, of 4.5 ± 1.7 K, is larger
 426 than most models simulate, so the models that match the ΔSSAT most closely would be the models
 427 with a larger ΔSSAT than average and thus also a larger ΔSIA. The only model that has a large SIA



428 reduction and not a good skill to match SSAT is EC-Earth, which features a PI simulation with far too
429 much sea ice, which allows an excessive LIG to PI Arctic warming. An additional result of our study
430 is that the mean Δ SSAT at the proxy locations is strongly correlated to Arctic-wide Δ SSAT north of
431 60° N in the models ($r=0.97$). Applying the regression relation between the two, implies that the mean
432 Δ SSAT at the proxy locations, of 4.5 K, is equivalent to an Arctic-wide warming at the LIG of 3.7 K.
433 This is thus a more representative value for the Arctic warming at the LIG, than using the simpler
434 proxy-location average.

435

436 The strong linear correlation between the magnitude of Δ SIA and Δ SSAT is applied to the proxy-
437 reconstructed Δ SSAT to give an estimate of the reduction of SIA from the PI to LIG of 4.4 mill. km²,
438 similar to that derived from our "best skill" approach. A similar value of 4.5 mill. km² is obtained
439 when extrapolating the method to Arctic-wide Δ SSAT north of 60° N. The models and data have
440 uncertainties, and the regressions applied are not between perfectly correlated quantities. However, it
441 is clear from both applied methods (each with two variants) that proxy-reconstructed Δ SSAT, in
442 combination with the model output, implies a larger sea ice reduction than the climatological multi-
443 model mean of 55%. It suggests a LIG SIA of ~ 1.3 mill. km², which is consistent with intermittently
444 ice-free summers – but with (low ice area) ice-present summers likely exceeding the number of ice-
445 free years. This result suggests that the fully-ice free HadGEM3 is somewhat too sensitive, and loses
446 summer sea ice too readily during the LIG, alongside that most other PMIP4 models are insufficiently
447 insensitive do not lose enough sea ice.

448

449 *Code availability.* Python code used to produce the manuscript plots is available on request from the
450 authors.

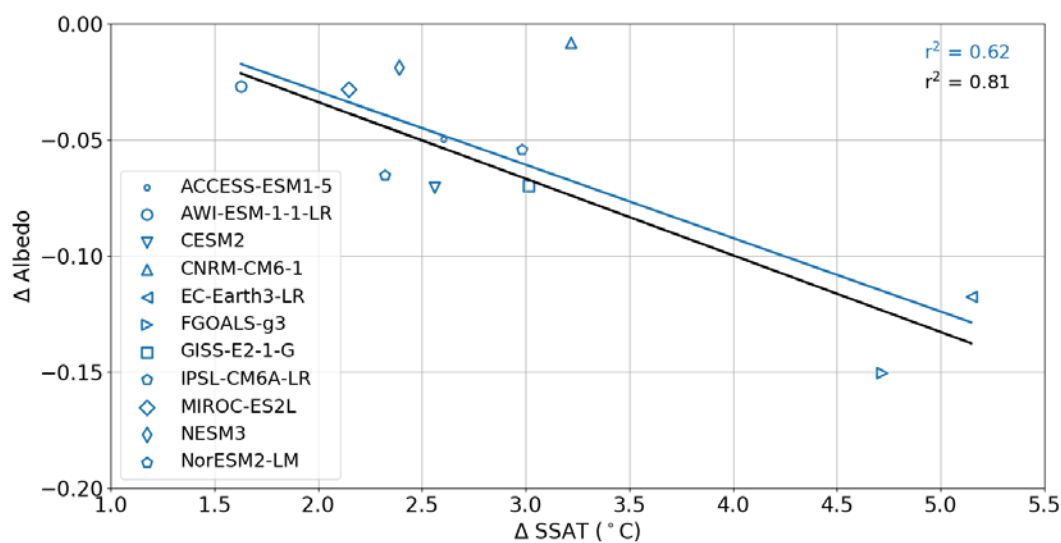
451

452 *Data availability.* The summer air temperature dataset is available at [https://data.bas.ac.uk/full-](https://data.bas.ac.uk/full-record.php?id=GB/NERC/BAS/PDC/01593)
453 [record.php?id=GB/NERC/BAS/PDC/01593](https://data.bas.ac.uk/full-record.php?id=GB/NERC/BAS/PDC/01593). All model data is available from the ESGF data node:
454 <https://esgf-node.llnl.gov/projects/esgf-llnl/>.

455



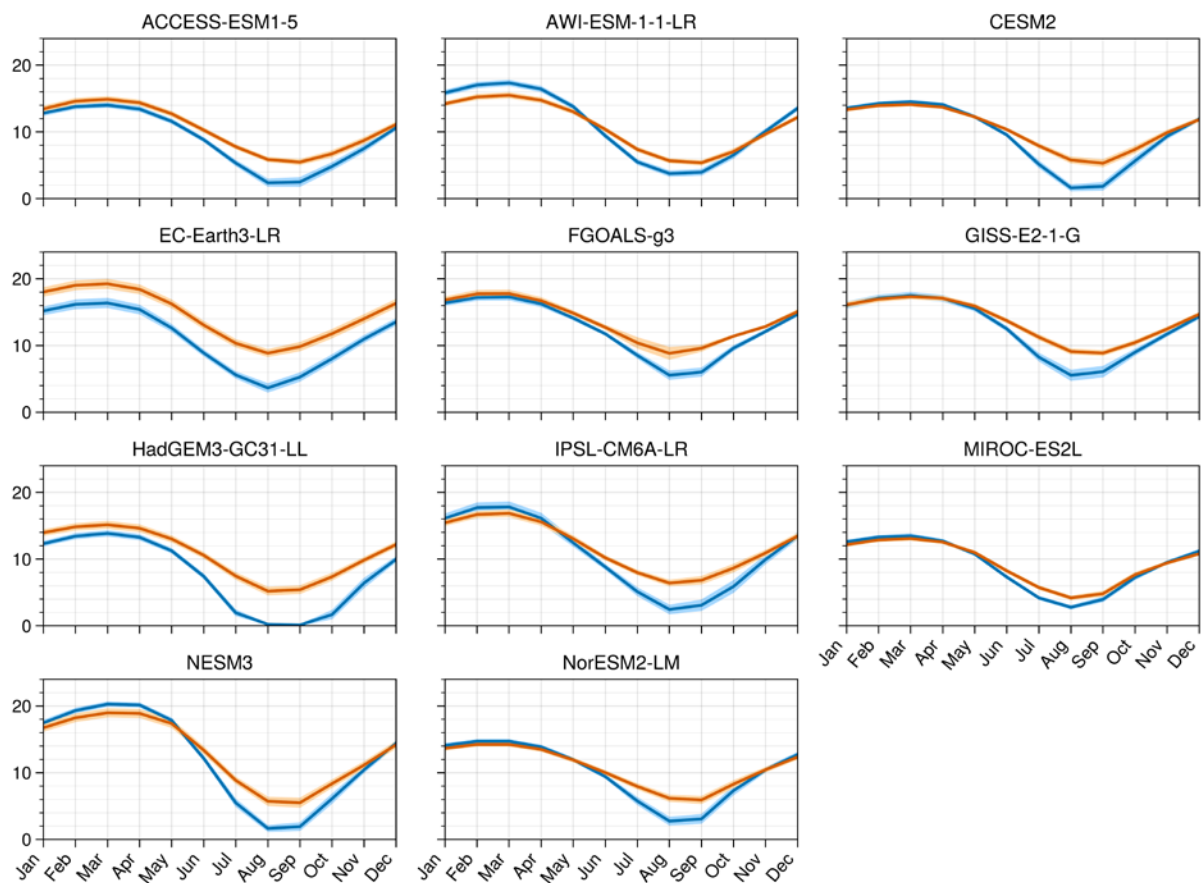
456 **Appendix**



457

458

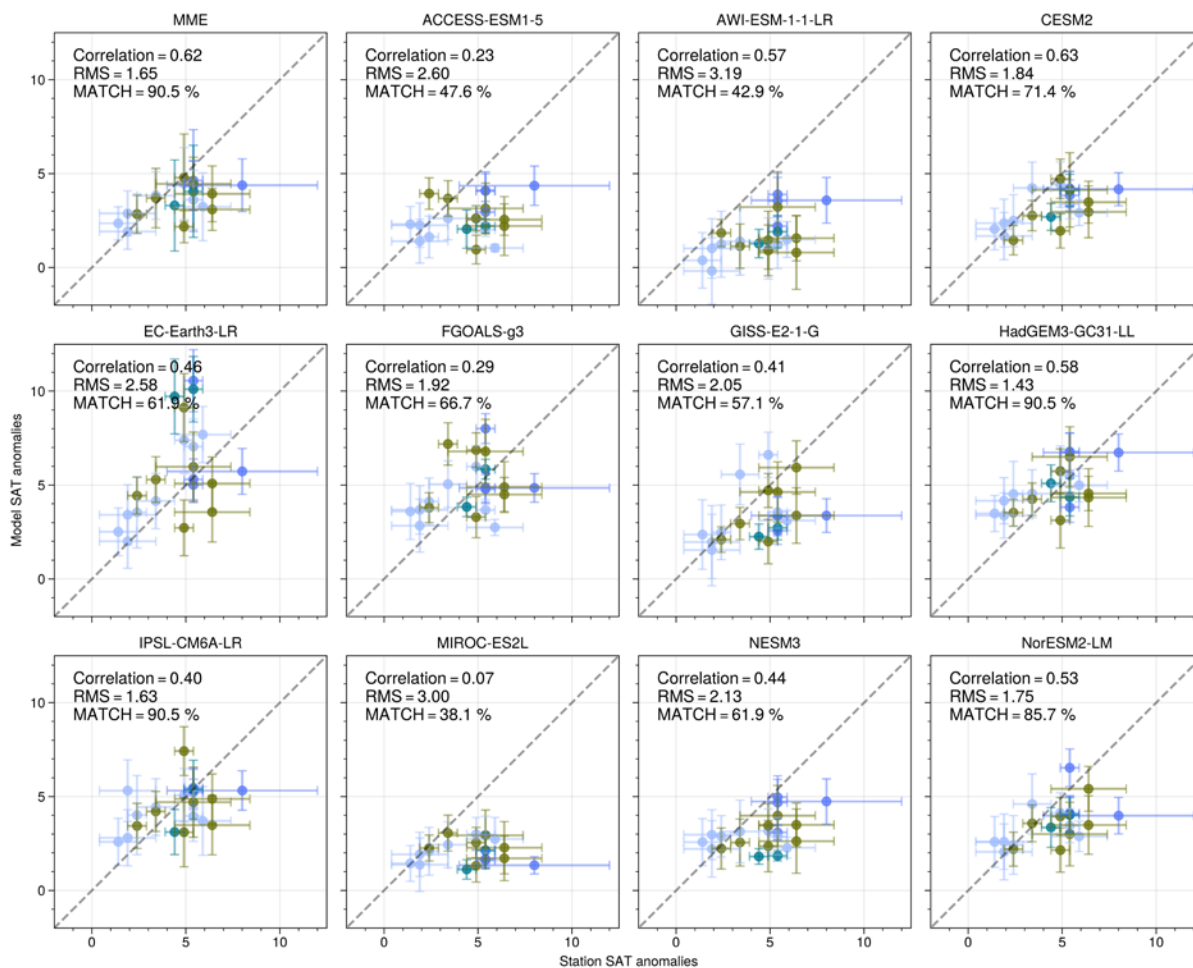
459 Figure A1. LIG-PI change in albedo over Arctic sea-ice as a function of LIG-PI change in SSAT ($^{\circ}$ C)
460 over the ice. The r^2 values and the linear fit lines are for the models including CNRM (blue) and
461 excluding CNRM (black). The CNRM model (upside triangle) is an outlier that influences the
462 strength rather than the nature of the correlation.



463

464 Figure A2. Sea ice area climatological seasonal cycle for each model.

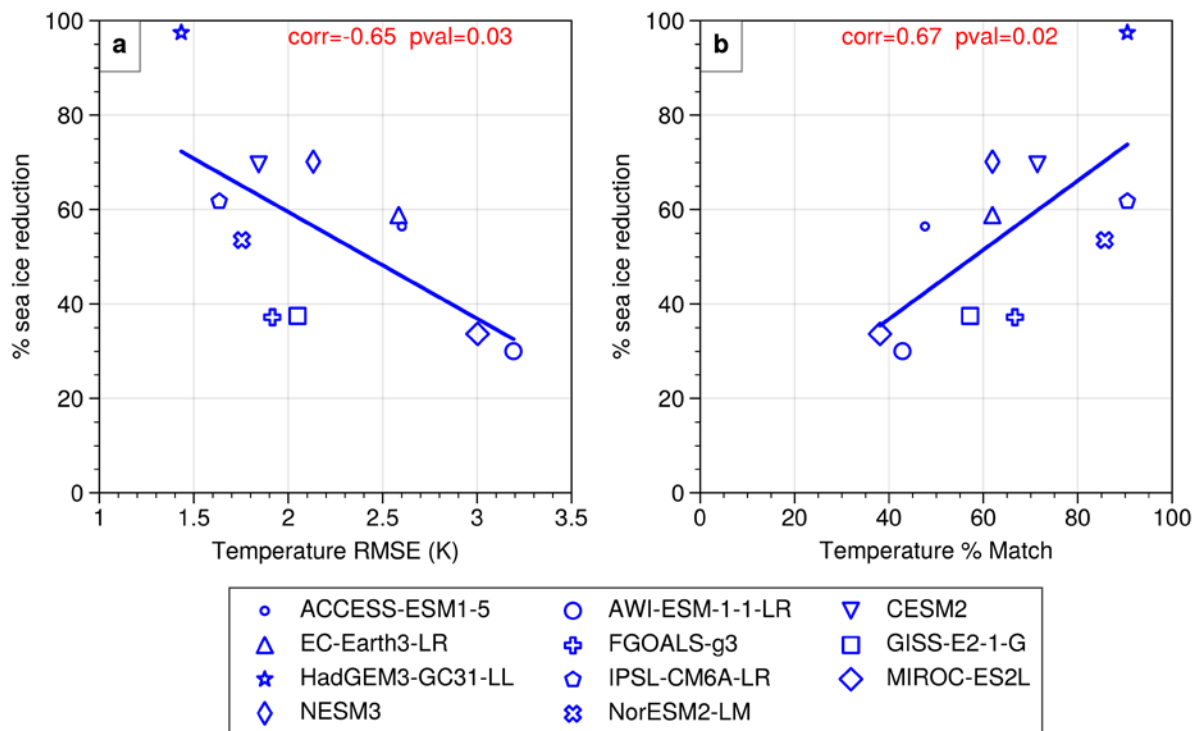
465



466 Figure A3. Modelled Δ SSAT versus proxy Δ SSAT. The scatter points show model data versus
467 observations for each proxy location. Error-bars represent one standard deviation on either side of the
468 proxy estimate. The correlation coefficients, between X and Y, RMSE and percentage matches with
469 observations for each model are indicated in each panel.

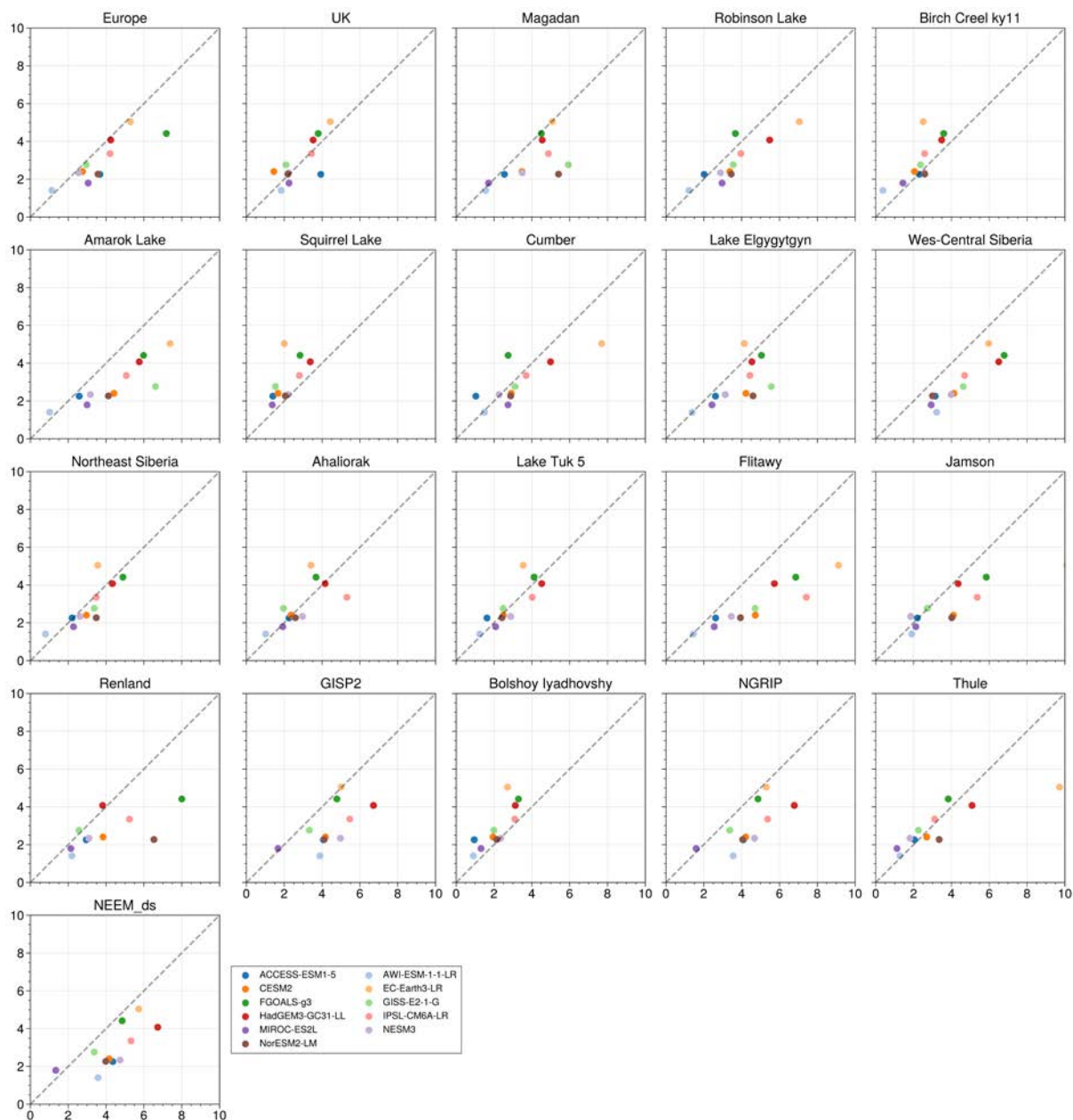


470



471

472 Figure A4: Modelled % sea ice area reduction from the LIG to the PI versus model skill to simulate
473 proxy Δ SSAT. a) The modelled %SIA reduction is scattered against the RMSE of the modelled
474 Δ SSAT compared to the proxy Δ SSAT for the 21 data locations. b) The modelled % SIA reduction
475 scattered against the percentage of Δ SSAT data points that the model can match (see methods).



476

477 Figure A5. Scatter Plot for climatological Δ SSAT at each observational location versus climatological
478 Δ SSAT averaged over entire Northern Hemisphere in each model



479 *Author contributions.* LCS planned and wrote the original draft. RS analysed model results and
480 prepared the figures. Figure 1 which was prepared by IVM. AdB wrote the second draft. MS
481 undertook additional analysis, checks and researched particular model results. All authors contributed
482 to the final text.

483

484 *Competing interests.* The authors have no competing interests.

485

486 *Acknowledgements.* LCS and RS acknowledge the financial support of NERC research grant
487 NE/P013279/1 and NE/P009271/1. LCS and IVM have received funding from the European Union's
488 Horizon 2020 research and innovation programme under grant agreement No 820970. AdB and MS
489 were supported by Swedish Research Council grant 2020-04791. This work used the ARCHER UK
490 National Supercomputing Service (<http://www.archer.ac.uk>) and the JASMIN analysis platform
491 (<https://www.ceda.ac.uk/services/jasmin/>).



492 **References**

- 493 Bartlein, P. J. and Shafer, S. L.: Paleo calendar-effect adjustments in time-slice and transient climate-
494 model simulations (PaleoCalAdjust v1.0): Impact and strategies for data analysis, *Geoscientific*
495 *Model Development*, 12, 3889–3913, 2019.
- 496 Berger, A. and Loutre, M.-F.: Insolation values for the climate of the last 10 million years, *Quaternary*
497 *Science Reviews*, 10, 297–317, 1991.
- 498 Bracegirdle, T. J., Colleoni, F., Abram, N. J., Bertler, N. A. N., Dixon, D. A., England, M., Favier, V.,
499 Fogwill, C. J., Fyfe, J. C., Goodwin, I., Goosse, H., Hobbs, W., Jones, J. M., Keller, E. D., Khan, A.
500 L., Phipps, S. J., Raphael, M. N., Russell, J., Sime, L., Thomas, E. R., van den Broeke, M. R., and
501 Wainer, I.: Back to the Future: Using Long-Term Observational and Paleo-Proxy Reconstructions to
502 Improve Model Projections of Antarctic Climate, *Geosciences*, 9,
503 <https://doi.org/10.3390/geosciences9060255>, 2019.
- 504 Cao, J., Wang, B., Yang, Y.-M., Ma, L., Li, J., Sun, B., Bao, Y., He, J., Zhou, X., and Wu, L.: The
505 NUIST Earth System Model (NESM) version 3: description and preliminary evaluation, *Geoscientific*
506 *Model Development*, 11, 2975–2993, <https://doi.org/10.5194/gmd-11-2975-2018>, 2018.
- 507 CAPE members: Last Interglacial Arctic warmth confirms polar amplification of climate change,
508 *Quaternary Science Reviews*, 25, 1383– 1400, 2006.
- 509 Capron, E., Govin, A., Stone, E. J., Masson-Delmotte, V., Mulitza, S., Otto-Bliesner, B., Rasmussen,
510 T. L., Sime, L. C., Waelbroeck, C., and Wolff, E. W.: Temporal and spatial structure of multi-
511 millennial temperature changes at high latitudes during the Last Interglacial, *Quaternary Science*
512 *Reviews*, 103, 116–133, <https://doi.org/10.1016/j.quascirev.2014.08.018>, 2014.
- 513 Capron, E., Govin, A., Feng, R., Otto-Bliesner, B. L., and Wolff, E. W.: Critical evaluation of climate
514 syntheses to benchmark CMIP6/PMIP4 127 ka Last Interglacial simulations in the high-latitude
515 regions, *Quaternary Science Reviews*, 168, 137–150, 2017.
- 516 Diamond, R., Sime, L. C., Schroeder, D., and Guarino, M.-V.: The contribution of melt ponds to
517 enhanced Arctic sea-ice melt during the Last Interglacial, *The Cryosphere Discussions*, 2021, 1–24,
518 <https://doi.org/10.5194/tc-2021-6>, 2021.



519 Fischer, H., Meissner, K. J., Mix, A. C., Abram, N. J., Austermann, J., Brovkin, V., Capron, E.,
520 Colombaroli, D., Daniau, A.-L., Dyez, K. A., et al.: Palaeoclimate constraints on the impact of 2 C
521 anthropogenic warming and beyond, *Nature geoscience*, 11, 474, 2018.

522 Govin, A., Capron, E., Tzedakis, P., Verheyden, S., Ghaleb, B., Hillaire-Marcel, C., St-Onge, G.,
523 Stoner, J., Bassinot, F., Bazin, L., Blunier, T., Combourieu-Nebout, N., Ouahabi, A. E., Genty, D.,
524 Gersonde, R., Jimenez-Amat, P., Landais, A., Martrat, B., Masson-Delmotte, V., Parrenin, F.,
525 Seidenkrantz, M.-S., Veres, D., Waelbroeck, C., and Zahn, R.: Sequence of events from the onset to
526 the demise of the Last Interglacial: Evaluating strengths and limitations of chronologies used in
527 climatic archives, *Quaternary Science Reviews*, 129, 1 – 36,
528 <https://doi.org/10.1016/j.quascirev.2015.09.018>, 2015.

529 Guarino, M. V., Sime, L., Schroeder, D., Lister, G., and Hatcher, R.: Machine dependence and
530 reproducibility for coupled climate simulations: the HadGEM3-GC3. 1 CMIP Preindustrial
531 simulation, *Geoscientific Model Development*, 13, 139–154, 2020a.

532 Guarino, M.-V., Sime, L. C., Schröder, D., Malmierca-Vallet, I., Rosenblum, E., Ringer, M., Ridley,
533 J., Feltham, D., Bitz, C., Steig, E. J., et al.: Sea-ice-free Arctic during the Last Interglacial supports
534 fast future loss, *Nature Climate Change*, pp. 1–5, 2020b.

535 IPCC: Climate Change 2013: The Physical Science Basis. Contribution of Working Group I to the
536 Fifth Assessment Report of the Intergovernmental Panel on Climate Change. [Stocker, T.F. and Qin,
537 D and Plattner, G and Tignor, M and Allen, S.K. and Boschung, J and Nauels, A and Xia, Y and Bex,
538 V and Midgley, P.M (eds.)], Tech. Rep. 5, Intergovernmental Panel on Climate Change, Cambridge,
539 United Kingdom and New York, NY, USA, <https://doi.org/10.1017/CBO9781107415324>, 2013.

540 IPCC: Climate Change 2021: The Physical Science Basis. Contribution of Working Group I to the
541 Sixth Assessment Report of the Intergovernmental Panel on Climate Change [Masson-Delmotte, V.,
542 P. Zhai, A. Pirani, S.L. Connors, C. Pean, S. Berger, N. Caud, Y. Chen, L. Goldfarb, M.I. Gomis, M.
543 Huang, K. Leitzell, E. Lonnoy, J.B.R. Matthews, T.K. Maycock, T. Waterfield, O. Yelekci, R. Yu,
544 and B. Zhou 385 (eds.)], Tech. Rep. 6, Intergovernmental Panel on Climate Change,
545 Cambridge, United Kingdom and New York, NY, USA, 2021.



546 Kageyama, M., Sime, L. C., Sicard, M., Guarino, M.-V., de Vernal, A., Stein, R., Schroeder, D.,
547 Malmierca-Vallet, I., Abe-Ouchi, A., Bitz, C., et al.: A multi-model CMIP6-PMIP4 study of Arctic
548 sea ice at 127 ka: sea ice data compilation and model differences, *Climate of the Past*, 17, 37–62,
549 2021.

550 Kaspar, F., Kühl, N., Cubasch, U., and Litt, T.: A model-data comparison of European temperatures
551 in the Eemian interglacial, *Geophysical Research Letters*, 32, 2005.

552 Lunt, D. J., Abe-Ouchi, A., Bakker, P., Berger, A., Braconnot, P., Charbit, S., Fischer, N., Herold, N.,
553 Jungclauss, J. H., Khon, V., et al.: A multi-model assessment of last interglacial temperatures, *Climate*
554 *of the Past*, 9, 699–717, 2013.

555 Malmierca-Vallet, I., Sime, L. C., Valdes, P. J., Capron, E., Vinther, B. M., and Holloway, M. D.:
556 Simulating the Last Interglacial Greenland stable water isotope peak: The role of Arctic sea ice
557 changes, *Quaternary Science Reviews*, 198, 1–14, 395
558 <https://doi.org/10.1016/j.quascirev.2018.07.027>, 2018.

559 Meehl, G. A., Senior, C. A., Eyring, V., Flato, G., Lamarque, J.-F., Stouffer, R. J., Taylor, K. E., and
560 Schlund, M.: Context for interpreting equilibrium climate sensitivity and transient climate response
561 from the CMIP6 Earth system models, *Science Advances*, 6, eaba1981,
562 <https://doi.org/10.1126/sciadv.aba1981>, 2020.

563 Notz, D. and the SIMIP Community: Arctic sea ice in CMIP6, *Geophysical Research Letters*, 47,
564 e2019GL086749, 2020.

565 Otto-Bliesner, B. L., Rosenbloom, N., Stone, E. J., McKay, N. P., Lunt, D. J., Brady, E. C., and
566 Overpeck, J. T.: How warm was the last interglacial? New model–data comparisons, *Philosophical*
567 *Transactions of the Royal Society A: Mathematical, Physical and Engineering Sciences*, 371,
568 20130097, 2013.

569 Otto-Bliesner, B. L., Braconnot, P., Harrison, S. P., Lunt, D. J., Abe-Ouchi, A., Albani, S., Bartlein, P.
570 J., Capron, E., Carlson, A. E., Dutton, A., et al.: The PMIP4 contribution to CMIP6–Part 2: Two
571 interglacials, scientific objective and experimental design for Holocene and Last 405 Interglacial
572 simulations, *Geoscientific Model Development*, 10, 3979–4003, 2017.



573 Otto-Bliesner, B. L., Brady, E. C., Zhao, A., Brierley, C., Axford, Y., Capron, E., Govin, A.,
574 Hoffman, J., Isaacs, E., Kageyama, M., Scussolini, P., Tzedakis, P. C., Williams, C., Wolff, E., Abe-
575 Ouchi, A., Braconnot, P., Ramos Buarque, S., Cao, J., de Vernal, A., Guarino, M. V., Guo, C.,
576 LeGrande, A. N., Lohmann, G., Meissner, K., Menviel, L., Nisancioglu, K., O’ishi, R., Salas Y Melia,
577 D., Shi, X., Sicard, M., Sime, L., Tomas, R., Volodin, E., Yeung, N., Zhang, Q., Zhang, Z., and
578 Zheng, W.: Large-scale features of Last Interglacial climate: Results from evaluating the *lig127k*
579 simulations for CMIP6-PMIP4, *Climate of the Past Discussions*, 2020, 1–41,
580 <https://doi.org/10.5194/cp-2019-174>, 2020.

581 Reynolds, R. W., Rayner, N. A., Smith, T. M., Stokes, D. C., and Wang, W.: An improved in situ and
582 satellite SST analysis for climate, *J. Climate*, 15, 1609–1625, 2002

583 Sime, L., Wolff, E., Oliver, K., and Tindall, J.: Evidence for warmer interglacials in East Antarctic ice
584 cores, *Nature*, 462, 342–345, 2009.

585 Turney, C. S. and Jones, R. T.: Does the Agulhas Current amplify global temperatures during super-
586 interglacials?, *Journal of Quaternary Science*, 25, 839–843, 2010.

587 Voltaire, A., Saint-Martin, D., Sénési, S., Decharme, B., Alias, A., Chevallier, M., Colin, J.,
588 Guérémy, J.-F., Michou, M., Moine, M.-P., et al.: Evaluation of CMIP6 deck experiments with
589 CNRM-CM6-1, *Journal of Advances in Modeling Earth Systems*, 11, 2177–2213, 2019.